scientific reports

Check for updates

OPEN

First record and integrative analysis of the invasive aphid *Cinara pilicornis* in South Korea

Minho Lee[1,2], Mariusz Kanturski[3], Min-Jung Kim[4], Andżela Glumac[3] & Seunghwan Lee[1,2,5]✉

This study presents the first record of the spruce shoot aphid, *Cinara pilicornis* (Hartig, 1841) (Hemiptera: Aphididae: Lachninae), in South Korea. Native to Europe, *C. pilicornis* has expanded its distribution globally and is recognized as a significant quarantine pest in South Korea, posing substantial ecological and economic risks to native spruce trees and forestry ecosystems. Through detailed morphological and molecular analyses, including scanning electron microscopy (SEM) and mitochondrial COI gene sequencing, the identity of *C. pilicornis* was confirmed. Phylogenetic analyses (BI and NJ) and species delimitation methods (ABGD, ASAP, and bPTP) further validated the species classification, with all South Korean populations belonging to haplotype 1 a putative ancestral haplotype widely distributed across other regions. Population analyses revealed limited genetic diversity in South Korea, suggesting a recent introduction. Climatic niche modeling indicated that *C. pilicornis* has the potential to establish populations in temperate and subtropical regions, including Europe, North America, coastal South America, and East Asia. Observations of colony behavior on *Picea abies* revealed high honeydew production and the formation of black sooty mold, causing visible damage to host plants. This study underscores the importance of strengthening quarantine measures and monitoring native spruce trees in national parks to mitigate the spread and impact of this invasive pest. Effective management strategies are essential to prevent further ecological disruption and economic losses caused by *C. pilicornis*.

Keywords Aphids, Quarantine pest, *Picea abies*, Morphology, COI, Distribution

Climate change, along with rising international trade and travel, is accelerating the spread of invasive pests[1–3]. These invasions cause significant damage to economically important food crops and trees and spread to harm native plants in the invaded country[3,4]. The genus *Cinara* Curtis, 1835 (Hemiptera: Aphididae: Lachninae) includes over 250 species distributed worldwide, all of which exhibit a strong host specificity for coniferous trees, particularly those within the Cupressaceae and Pinaceae[5–8]. *Cinara* species possess significant potential for intercontinental dissemination facilitated by the dynamic international trade among countries and continents, driven by the plantation of plants[9]. The spruce shoot aphid, *Cinara pilicornis* (Hartig, 1841) feeds on *Picea* spp. and *Tsuga heterophylla*[10]. A key symptom of aphid infestation is the yellowing of the host plant's leaves, along with the production of honeydew that leads to black sooty mold on shoots and leaves[7]. Native to Europe, this aphid has been expanding its distribution to other regions, such as Japan[11], Australia[12], North and South America[13], Kazakhstan and India[14], New Zealand[15], China[16], Argentina[17], Turkey[18], and Russia[19]. The Animal and Plant Quarantine Agency of South Korea has designated this species as a quarantine pest, implementing stringent measures to regulate and monitor imported crops and trees from neighboring countries[20].

In this study, we report the first record of the spruce shoot aphid, *C. pilicornis*, in South Korea. The research has three primary objectives: (1) to monitor and identify the spruce shoot aphid feeding on spruce trees in South Korea through detailed morphological and molecular analyses. For accurate species identification, we provided ecological photographs and detailed redescriptions of both apterous and alate viviparous females. Morphological characteristics, including sensilla structure, were examined using light microscopy and scanning

[1]Insect Biosystematics Laboratory, Department of Agricultural Biotechnology, Seoul National University, Seoul 08826, Korea. [2]Research Institute of Agricultural and Life Sciences, Seoul National University, Seoul 08826, Korea. [3]Institute of Biology, Biotechnology and Environmental Protection, Faculty of Natural Sciences, University of Silesia in Katowice, Bankowa 9, Katowice 40–007, Poland. [4]Forest Entomology and Pathology Division, National Institute of Forest Science, Seoul 02455, Korea. [5]Division of Entomology, College of Agriculture and Life Sciences, Seoul National University, Gwanak-ro 1, Gwanak-gu, Seoul 08826, Korea. ✉email: seung@snu.ac.kr

electron microscopy (SEM). For molecular identification, genetic divergences and species delimitation were conducted using phylogenetic analyses derived from COI sequence data. (2) to conduct population analysis using TCS network and principal coordinates analysis (PCoA) to infer the invasion route of this species. (3) to estimate the global potential distribution of *C. pilicornis* by assessing its climatic suitability.

Results

Apterous viviparous female– redescription

Figures 1 d, e and 2 and S Table 1.

Color. In life: head, thorax, and abdomen orange-brown dusted with white wax (Fig. 1 d, e). Eyes black. ANT I-V light brown. ANT VI brown. Femora dusky brown. Tibiae brown with darker basal and apical part. Tarsi dark brown. SIPH reddish brown. **Pigmentation in mounted specimens**: head and thorax brown. Abdomen light brown. ANT I-VI light brown. ANT VI light brown with 1/2 distal end brown. Femora dusky brown. Tibiae brown with darker basal and apical part. Tarsi dark brown. SIPH brown. Cauda brown and GP brown (Fig. 2a). **Morphometric characters**: body elongated oval (Fig. 2a). HW 0.57–0.66 × ANT. ANT 0.34–0.41 × BL. ANT III with 0–2 secondary rhinaria, shorter than ANT IV + V + VI (Fig. 2f). ANT IV shorter than ANT V with 0–2 secondary rhinaria. ANT V a little longer than ANT VI with one rounded primary rhinarium with one small rounded secondary rhinaria. ANT VI with PT 0.20–0.29 × BASE, with one rounded primary rhinarium and 4–5 accessory rhinaria. Other antennal ratios: VI/III 0.39–0.53, V/III 0.44–0.59, IV/III 0.34–0.41. Longest setae of ANT III 3.32–4.95 × basal diameter of ANT III. Rostrum reaches ABD III–IV. URS 0.84–1.03 × ANT III, 1.85–2.22 × ANT VI and 0.77–0.90 × HT II with 6 fine accessory setae (Fig. 2e). TIBIAE III covered with long fine setae on dorsal side longer (0.19–0.20 mm) than the width of TIBIAE III at midpoint (Fig. 2 g). HT I basal length 1.05–1.33 × dorsal, 0.38–0.46 × ventral. HT II 1.06–1.20 × ANT III and 2.12–2.71 × ANT VI. HT II sickle-shaped (Fig. 2b). ABD VIII in form of broken band and few small sclerites with 24–47 setae. SIPH cone 3.03–4.05 × SIPH pore (Fig. 2c). GP U-shaped with 26–38 fine setae (Fig. 2 d). Cauda semi-circular with many long (0.15–0.17 mm), fine, pointed setae.

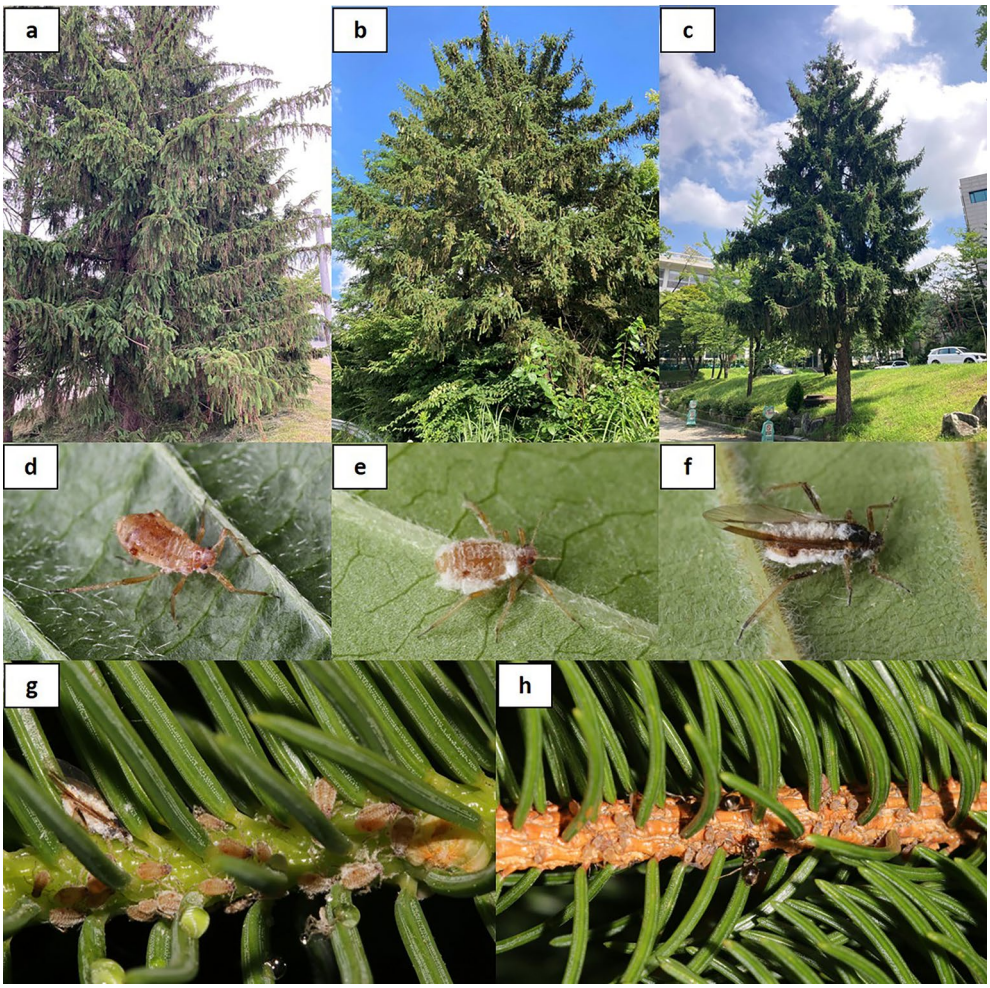

Fig. 1. *Cinara pilicornis*. (**a**-**c**) host plant (*Picea abies*); (**d**) apterous viviparous female; (**e**) apterous viviparous female (wax form); (**f**) alate viviparous female; (**g**) colony on host plant (in spring); (**h**) colony on host plant (in summer).

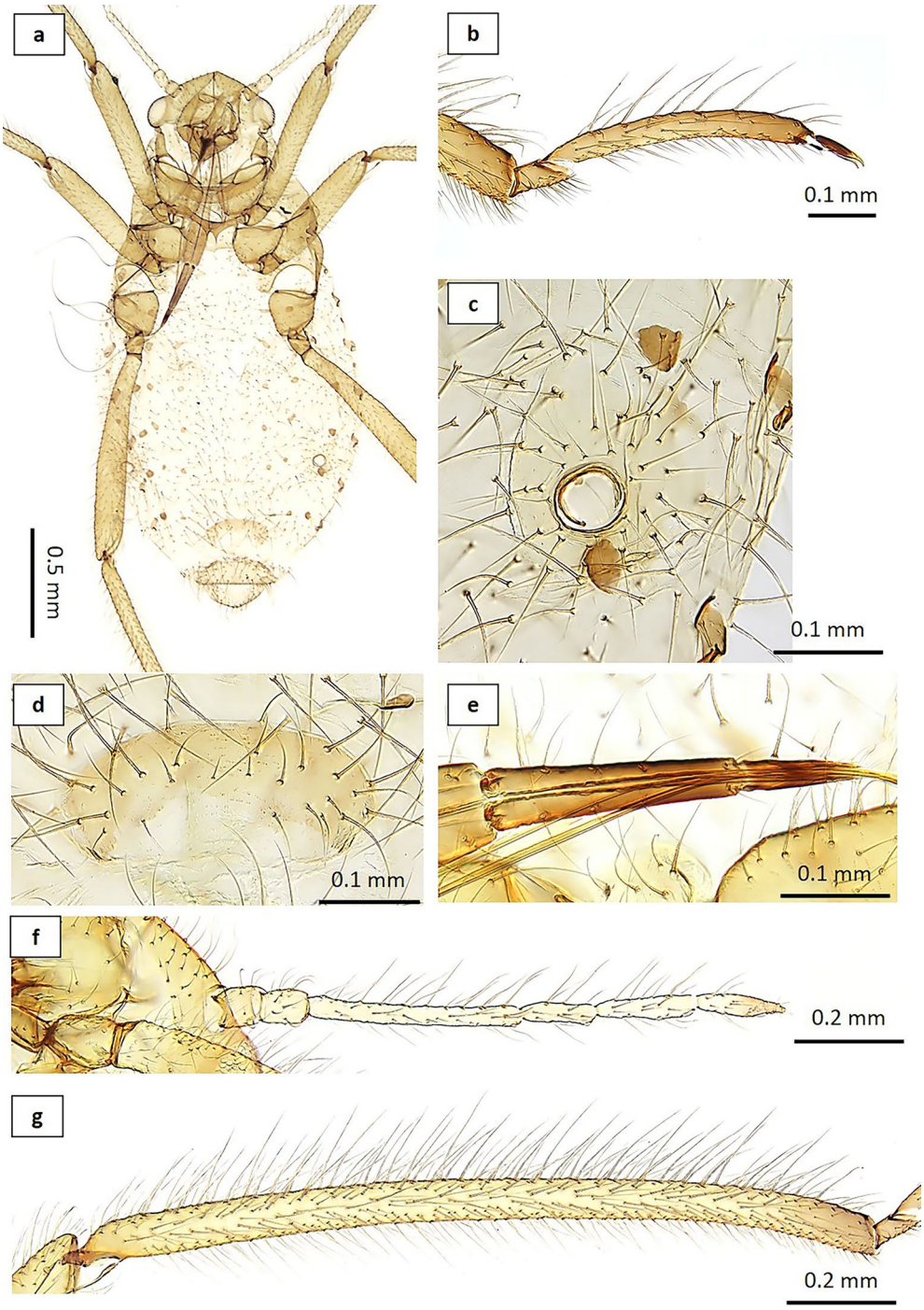

Fig. 2. *Cinara pilicornis*, apterous viviparous female: (**a**) body, (**b**) second segment of hind tarsus (HT II), (**c**) siphunculi (SIPH), (**d**) genital plate (GP), (**e**) ultimate rostral segment (URS), (**f**) antennae (ANT), (**g**) hind tibiae (TIBIAE III).

Alate viviparous female – redescription

Figures 1f and 3 and S Table 1.

Color. In life: head, thorax, and abdomen brown dusted with white wax. Eyes black. ANT I and II brown. ANT III light brown with 4/5 distal end brown. ANT IV–VI light brown with 3/4 distal end brown. Femora dusky dark brown. Tibiae brown with darker basal and apical part. Tarsi dark brown. SIPH dark brown. Fore, hind wings marked with slight fuscous (Fig. 1f). **Pigmentation in mounted specimens**: head and thorax brown. Abdomen light brown. ANT I and II brown. ANT III light brown with 1/3 distal end brown. ANT IV–V light brown with 1/2 distal end brown. ANT VI light brown with 3/4 distal end brown. Femora dusky brown. Tibiae brown with darker basal and apical part. Tarsi dark brown. SIPH brown. Cauda brown and genital brown (Fig. 3a). **Morphometric characters**: body elongated oval (Fig. 3a). HW 0.55–0.57 × ANT. ANT 0.37–

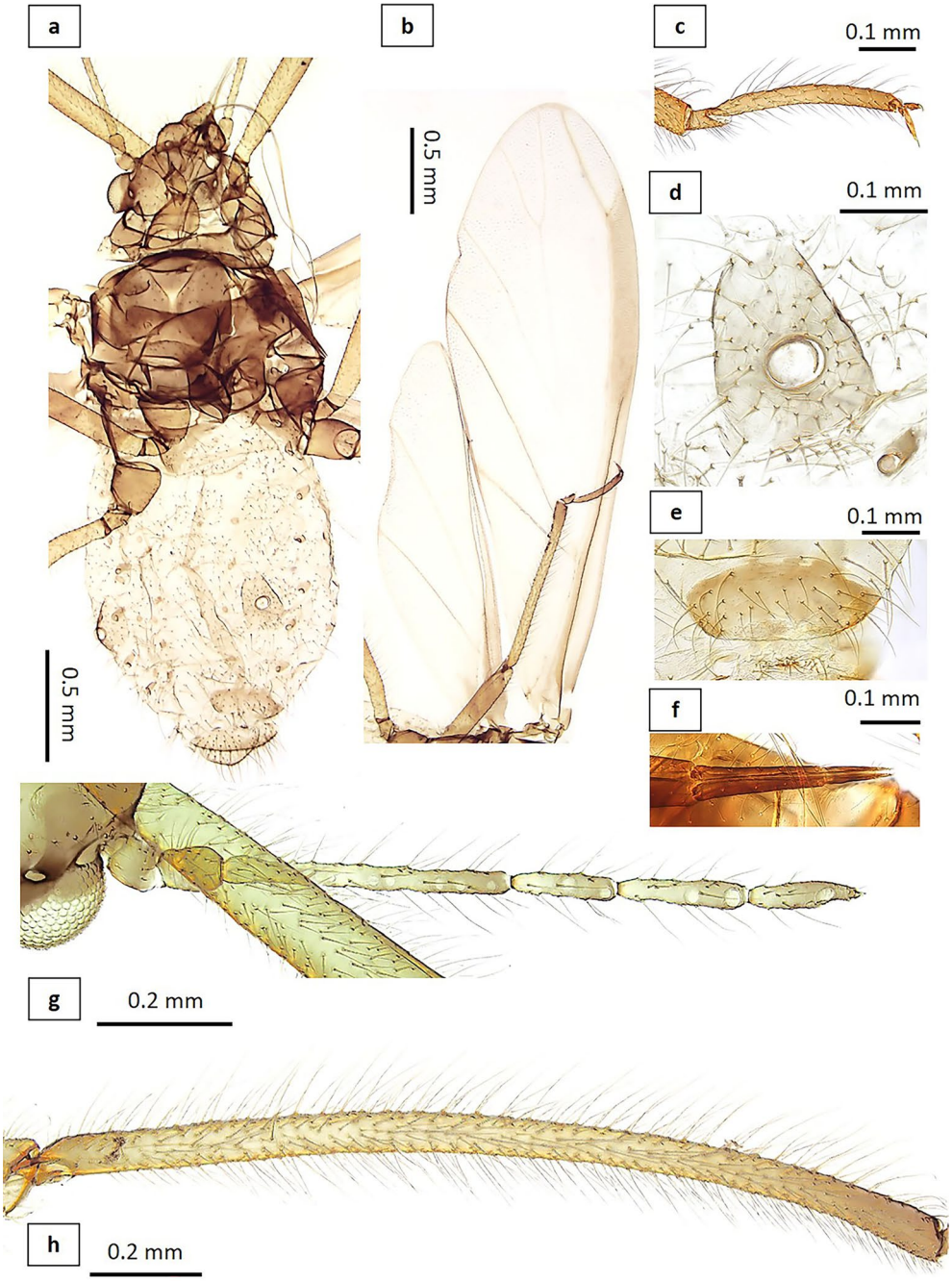

Fig. 3. *Cinara pilicornis*, alate viviparous female: (**a**) body, (**b**) wing, (**c**) second segment of hind tarsus (HT II), (**d**) siphunculi (SIPH), (**e**) genital plate (GP), (**f**) ultimate rostral segment (URS), (**g**) antennae (ANT), (**h**) hind tibiae (TIBIAE III).

0.40 × BL. ANT III with 5–7 secondary rhinaria, shorter than ANT IV + V + VI. ANT IV shorter than ANT V with one secondary rhinarium. ANT V longer than ANT VI with one rounded primary rhinarium with one small rounded secondary rhinarium (Fig. 3g). ANT VI with PT 0.22–0.25 × BASE, with one rounded primary rhinarium and 4–5 accessory rhinaria. Other antennal ratios: VI/III 0.37–0.42, V/III 0.42–0.48, IV/III 0.35–0.38. Longest setae of ANT III 4.10–4.22 × basal diameter of Ant III. Rostrum reaches ABD III. URS 0.76–0.81 × ANT III, 1.90–2.05 × ANT VI and 0.75–0.76 × HT II with 6 fine accessory setae (Fig. 3f). TIBIAE III covered with long and fine setae on dorsal side longer (0.20–0.22 mm) than the width of TIBIAE III at midpoint (Fig. 3h). HT I basal length 1.09–1.34 × dorsal, 0.39–0.47 × ventral. HT II 1.01–1.07 × ANT III and 2.55–2.71 × ANT VI. HT II sickle-shaped (Fig. 3c). ABD VIII in form of broken band and few small sclerites with 29–31 setae. SIPH cone 4.13–5.22 × SIPH pore (Fig. 3d). GP U-shaped with 27–33 fine setae (Fig. 3e). Cauda semi-circular with many long (0.14–0.15 mm), fine, pointed setae. Fore wings with media branched twice (Fig. 3b).

Notes on SEM morphology and sensilla of apterous viviparous female

General characters

The body and appendages of apterous viviparous females of *C. pilicornis* are densely covered with very long, fine (hair-like) trichoid sensilla (setae) which in a general view seem to have very thin, pointed apices (Fig. 4a). Compound eyes are well-developed, rounded, protuberant and consist of many facets (single ommatidia) which are regularly arranged. In the lower, hind part of the compound eyes, a well-developed triommatidium on an ocular tubercle is visible (Fig. 4a, b). Apterous viviparous females of *C. pilicornis* are characterized by legs with normal two-segmented tarsi, which are densely covered with setae, equipped by two pointed claws and clearly visible parempodia (Fig. 4c, d). The abdomen bears many long, pointed setae, and is characterized by a shortened cauda with the remaining perianal structures (ABD VIII and anal plate). The chaetotaxy is adapted for ant attendance, which is clearly visible in the lateral view (Fig. 4e) as described in previous studies[21–23]. The shortened cauda and very long setae are also visible at the end of the dorsal abdomen (Fig. 4 h) as well as from the ventral view (Fig. 4i). SIPH are rather low, characterized by a well-developed flange, and are lying on rounded or oval, protuberant sclerites, which are covered with 38–42 setae of the same length (Fig. 4f, g).

Antennal sensilla

The antennal segments of apterous viviparous females of *C. pilicornis* bear many sensilla including the secondary rhinaria. All segments are covered with long, fine, and (in the general view) pointed type I trichoid sensilla (setae) and the pedicel additionally bears two other kinds of sensilla. The dorso-lateral side of the pedicel bears a single campaniform sensilla (Fig. 5a), whilst on the ventro-lateral side two rhinariola may be noted (Fig. 5b). Flagellar segments III-V besides the trichoid sensilla bear small multiporous placoid sensilla (secondary rhinaria), and the fifth antennomere moreover bears one large multiporous sensillum at the distal end (Fig. 5c, d). The last antennal segment is the richest in these structures and besides type I trichoid sensilla, type II trichoid sensilla, large and small multiporous placoid sensilla and sunken coeloconic sensilla were observed (Fig. 5e). The pedicel campaniform sensillum is rounded or oval, 11.00–12.50 µm in diameter, with a wide collar and a rounded cap, 4.00–4.70 µm in diameter with a slightly laterally situated pore (Fig. 5f, g). The rhinariola are in the form of two single openings with sensilla pegs (probably type I sunken coeloconic sensilla). One opening

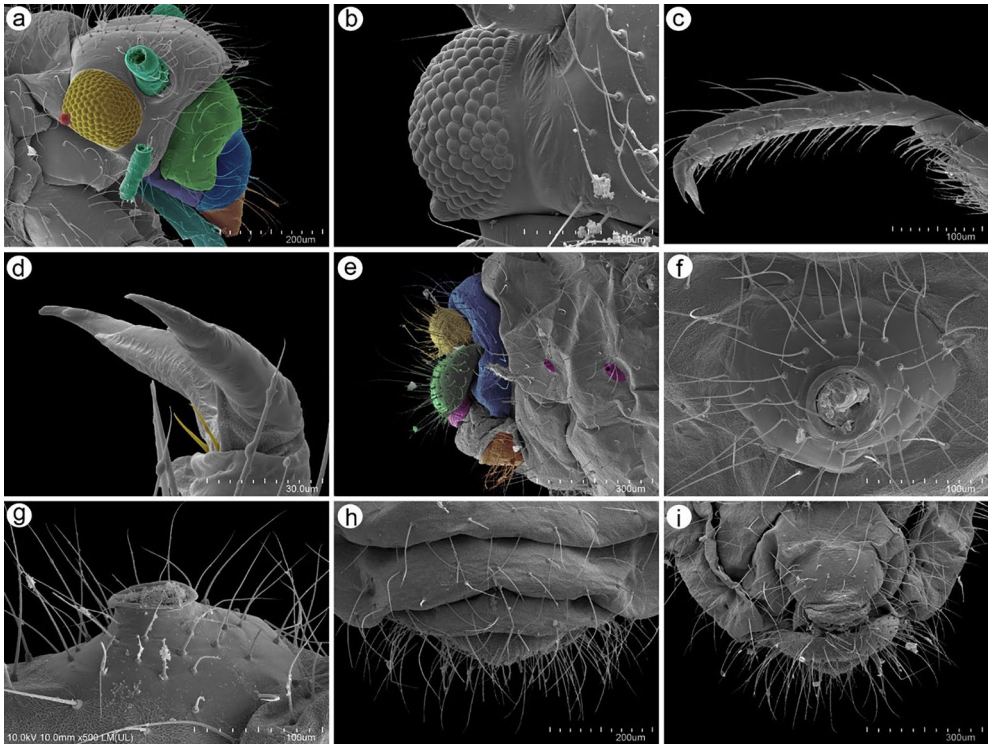

Fig. 4. General morphological characters of apterous viviparous female of *C. pilicornis*. (**a**) lateral side of the head showing compound eyes (yellow) with an ocular tubercle (red), antennal segments I and II (patina) and the mouthparts like large mandibular lamina (green) covering the maxillary lamina (violet), postclypeus (blue), anteclypeus (orange) and the basal segments of the labium (turquoise), (**b**) part of the dorsal side of the head with trichoid sensilla and compound eye with the ocular tubercle, (**c**) hind tarsus, (**d**) distal end of second segment of hind tarsus (HT II) with relatively long parempodia (yellow), (**e**) lateral side of the end of the abdomen showing the spiracles (purple), ABD VIII (blue), cauda (yellow), anal plate (green), rudimentary gonapophyses (lilac) and genital plate (orange), (**f**) siphunculus dorsal view, (**g**) siphunculus lateral view), (**h**) dorsal end of abdomen showing ABD VIII and part of cauda, (**i**) ventral side of abdomen showing part of the cauda, anal plate, rudimentary gonapophyses and genital plate.

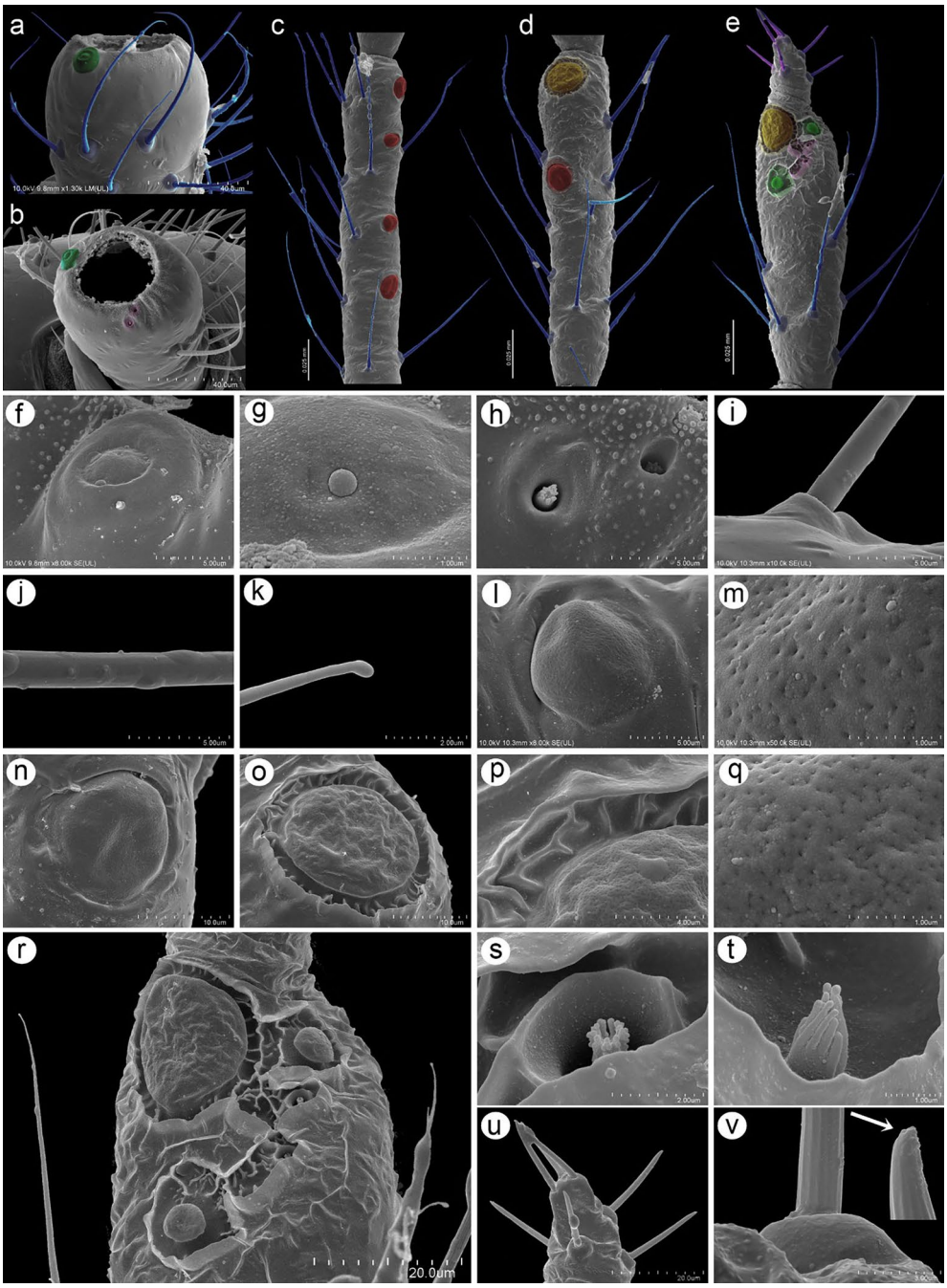

is about 1.90–1.95 µm in diameter and the protruding sensillum bears about six main projections which are additionally divided into 2–3 rounded apices. The second opening is about 1.30–1.35 µm in diameter and the hidden sensillum has seven visible projections which are single or only divided into two rounded apices (Fig. 5h). Type I trichoid sensilla are tubular, arise from flexible sockets at an angle of about 45°, and are trapezoid in the lateral view (Fig. 5i). The sensilla are moreover characterized by a smooth surface on the basal part, but later delicate and rather poorly-visible longitudinal ribbing is visible (Fig. 5i, j). Examination of their apices under high magnification revealed that (in the general view) pointed apices are in fact very slightly capitate (Fig. 5k). Small multiporous placoid sensilla (secondary rhinaria) are mostly rounded and slightly protuberant, 9.30–14.00 µm in diameter. They are mostly surrounded by a small cuticular collar, which in some cases is almost invisible (Fig. 5l, n). The membrane of the small placoid sensilla is characterized by relatively clearly, rounded pores, 15–20 per μm^2 (Fig. 5m). In contrast, the large multiporous placoid sensillum on antennal segment V is flatter, surrounded with a clearly visible cuticular collar with transverse reinforcements, and is 18.00–19.00 µm in diameter (Fig. 5o, p). The membrane of the large sensillum is characterized by clearly more densely arranged pores which are additionally more oval, 30–40 per μm^2 (Fig. 5q). The main group of sensilla of the last antennal segment lie in the distal part of the base and consist of the large multiporous placoid sensillum (major rhinarium), two small multiporous placoid sensilla in polar positions and four sunken coeloconic sensilla of two types between them (all these six sensilla are the accessory rhinaria). The large multiporous placoid sensillum is almost of the same characters as the sensillum on the distal part of the penultimate segment, 18.50–19.50 µm in diameter.

◀**Fig. 5**. Antennal sensilla of apterous viviparous female of *C. pilicornis*. (**a**) dorsal side of pedicel with type I trichoid sensilla and campaniform sensillum (green), (**b**) upper side of pedicel showing the campaniform sensillum (green) on the dorsal side and two rhinariola (pink) on the ventral side, (**c**) part of antennal segment III with type I trichoid sensilla (blue) and small multiporous placoid sensilla (red), (**d**) antennal segment V with type I trichoid sensilla (blue) one small multiporous placoid sensillum (red) and large multiporous placoid sensillum (yellow), (**e**) antennal segment VI with type I trichoid sensilla on the basal part (blue), type II trichoid sensilla on the terminal process (purple), large multiporous placoid sensillum (yellow) – major rhinarium, two small multiporous placoid sensilla (green) and four sunken coeloconic sensilla of two types (pink) – accessory rhinaria, (**f**) structure of the pedicel campaniform sensillum, (**g**) ultrastructure of the campaniform sensillum cap with the pore covered by an artifact, (**h**) ultrastructure of the pedicel rhinariola, (**i**) ultrastructure of the socket and basal part of type I trichoid sensillum, (**j**) ultrastructure of the medial surface of type I trichoid sensillum, (**k**) ultrastructure of the apical end of type I trichoid sensillum, (l) structure of the small multiporous placoid sensillum on antennal segment III (secondary rhinarium), (**m**) ultrastructure of the porous membrane of the small placoid sensillum, (**n**) structure of the small multiporous placoid sensillum on ANT V, (**o**) structure of the large multiporous placoid sensillum on antennal segment V, (**p**, **q**) ultrastructure of the porous membrane of the large multiporous placoid sensillum on antennal segment V, (**r**) arrangement of the sensilla on antennal segment VI with large multiporous placoid sensillum, two small multiporous placoid sensilla lying diagonally and in polar positions between which four sunken coeloconic sensilla are visible, (**s**) ultrastructure of the type I coeloconic sensillum, (**t**) ultrastructure of the type II coeloconic sensillum, (**u**) type II trichoid sensilla (apical and subapical setae) on the tip of the terminal process, (**v**) ultrastructure of the type II trichoid sensillum socket, surface and apical end (arrow).

The sensilla known as accessory rhinaria lie in a slightly crescent-shaped line obliquely to the major rhinarium (Fig. 5r). Small multiporous placoid sensilla on the last antennal segment are always smaller, 5.50–6.50 µm and different in size (mushroom-shaped) in contrast to the small multiporous placoid sensilla on ANT III-V (accessory rhinaria). The two types of sunken coeloconic sensilla are characterized by two type I coeloconic sensilla which are more hidden, surrounded by an elevated collar and ten very short major projections which have single, double or triple, spherical apices (Fig. 5 s). On the other hand the type II coeloconic sensilla lie in a wide, bowl-shaped cavity surrounded by a cuticular collar and are characterized by 10–12 long projections with capitate apices (Fig. 5 t). The type II trichoid sensilla are located on the distal part of the terminal process of the last antennal segment and are clearly divided into three so-called apical setae and 4–5 lower-lying subapical setae (Fig. 5u). They are approximately 11.50–17.50 µm in length, arise from in flexible rounded sockets, are characterized by well-developed ribbing on their whole length and have tattered apices (Fig. 5v).

Mouthpart sensilla

The labium of *C. pilicornis* is mostly covered with type I trichoid sensilla and characterized by long, narrow, pointed ultimate rostral segments (URS or IV + V). Sensilla cover the whole length and each side of the segment IV (Fig. 6a). The border between rostral segments IV and V bears three pairs of long, fine, pointed trichoid sensilla (primary setae), one pair on the ventral, one pair at the lateral side and one pair on the dorso-lateral side (Fig. 6a, b). The apex of the last rostral segment bears rather long type III basiconic sensilla (Fig. 6b, c). On the basal part of segment IV, one pair of type II basiconic sensilla can be noted (Fig. 6 d). The type II basiconic sensilla are about 24.00–26.00 µm in length, arise from flat, rounded, flexible sockets, are smooth at the very basal part, then ribbed on the rest of their length (Fig. 6e) and have rounded apices (Fig. 6f). Trichoid sensilla along the rostral segments and especially the fourth segment are identical to the antennal sensilla, long, fine and pointed in the general view (Fig. 6 g). Also similarly, they arise from flexible sockets and are smooth on the very basal part but then become ribbed (Fig. 6 h). The last rostral segment bears about seven pairs of rather long, smooth type III basiconic sensilla, 5.50–6.50 µm long (Fig. 6i). The sensilla are located on each side of the segment apical end, arising from inflexible, flat or slightly recessed sockets (Fig. 6j), and have rounded apices (Fig. 6k).

Leg and body surface sensilla

The legs, like other parts of the body of *C. pilicornis*, are very densely covered with long, fine, pointed trichoid sensilla over their whole length and surfaces (Fig. 7a), but besides them, campaniform sensilla may also be found on the inner side of the trochanter (two) and proximal bases of the femora (six) (Fig. 7b). The campaniform sensilla on the legs are rounded, on the trochanter they are of the same size but on the femur they form two groups of three larger (ca. 6.00–7.50 µm in diameter) and three smaller (ca. 4.25–5.00 µm in diameter) ones (Fig. 7c). The general structure of the campaniform sensillum is built from a slightly elevated collar and flat cap with an almost always centrally placed pore (Fig. 7 d). Only one campaniform sensillum is different from the other ones and is characterized by an elevated, pointed cap (Fig. 7e), which so far has been observed in some campaniform sensilla on aphids wings. The trichoid sensilla covering the femora and tibiae are arranged regularly over the whole surface of the cuticle (Fig. 7f), arising from flexible, trapezoid (in lateral view) sockets at an angle of about 45°, and are smooth on the basal part (Fig. 7 g) and slightly ribbed on their further length (Fig. 7 h). Besides the trochanter and femora, campaniform sensilla may be found on the dorsal sides of distal HT I and proximal HT II (Fig. 7i), and their general structure is similar to that previously described for campaniform sensilla. The campaniform sensillum on the HT I is the most different from the other ones due to the large cap and narrow collar (Fig. 7j) while the one on HT II is more similar to those on the trochanter and femur and their pores are shifted nearer the cap edge (Fig. 7k). The parempodia in the examined specimens seem to be relatively

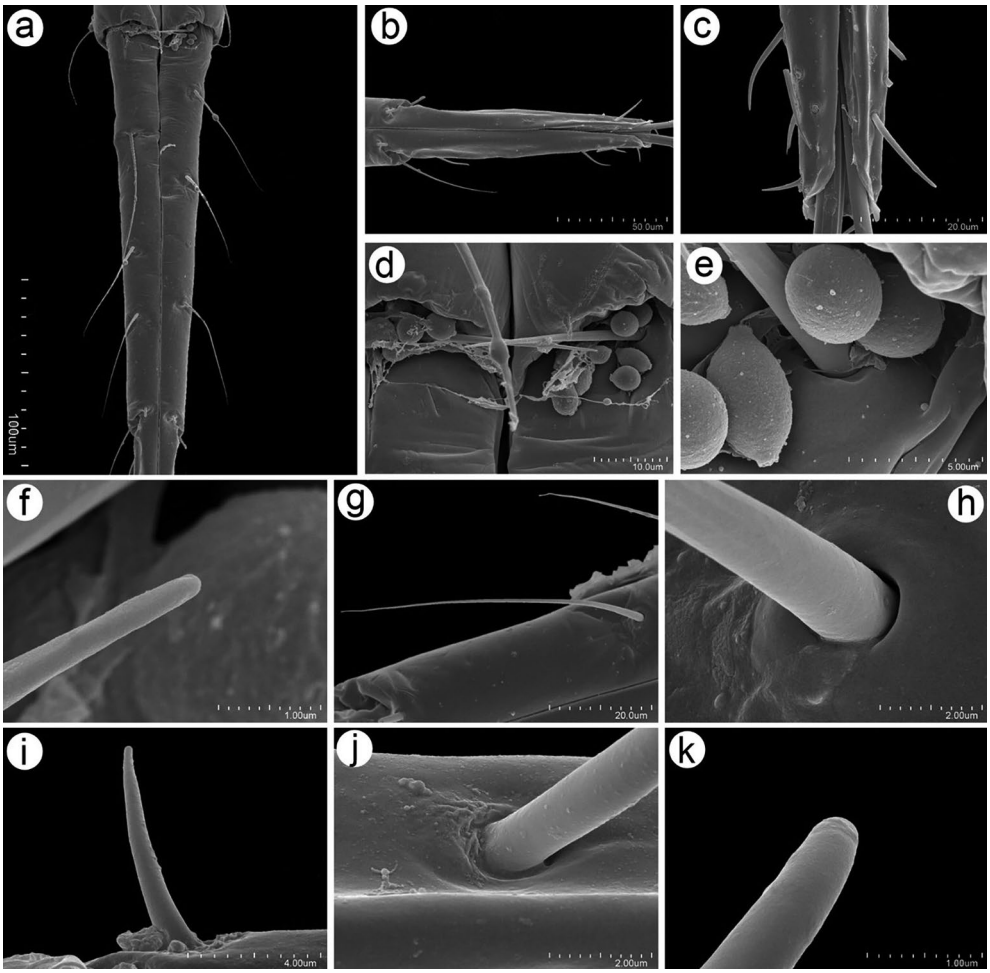

Fig. 6. Mouthparts sensilla of apterous viviparous female of *C. pilicornis*. (**a**) labial segment IV with visible trichoid sensilla, (**b**) labial segment V with three pairs of trichoid sensilla on the border with the labial segment IV and type III basiconic sensilla, (**c**) type III basiconic sensilla and stylets, (**d**) type II basiconic sensilla on the basal part of labial segment IV, (**e**) ultrastructure of the type II basiconic sensilla socket and sensillum surface, (**f**) apical end of type II basiconic sensillum, (**g**) structure of the trichoid sensillum, (**h**) ultrastructure of the trichoid sensillum socket and surface with molting pore, (**i**) structure of type II basiconic sensillum, (**j**) ultrastructure of the socket of the type II basiconic sensillum, (**k**) ultrastructure of the apical end of the type II basiconic sensillum.

long for Lachninae, being 13.00–14.50 µm in length, tubular and pointed (Fig. 7l). The cuticle surface structure varies depending of the body part. On the head, the cuticle is generally smooth or only here and there slightly wrinkled (Fig. 7m) and covered with trichoid sensilla of the same characters as those on the antennae and mouthparts, with more protuberant sockets (Fig. 7n). After a deeper examination under higher magnification the head cuticle appears to be covered with very small, rounded, oval depressions which may be very poorly secreting or inactive wax glands (Fig. 7o). In contrast to the head, the dorsal abdominal cuticle is clearly different, forming very densely polygonal microsculpture (Fig. 7p, q) but the sensilla are of the same characters and structure, sometimes with slightly narrower and more elevated sockets (Fig. 7r). Deeper examination in higher magnification revealed that the surface of the abdominal cuticle bears numerous very small, rounded, stump-shaped structures (Fig. 7s, t), which taking into account that the alive specimens are covered by wax secretions must be recognized as the wax gland. The lateral side of the abdomen is characterized by the same features of the cuticle, trichoid sensilla (Fig. 7u) and numerous very small wax glands (Fig. 7v-x).

Key to
Cinara
species feeding on
Picea abies (Modified following the latest digital update[7].

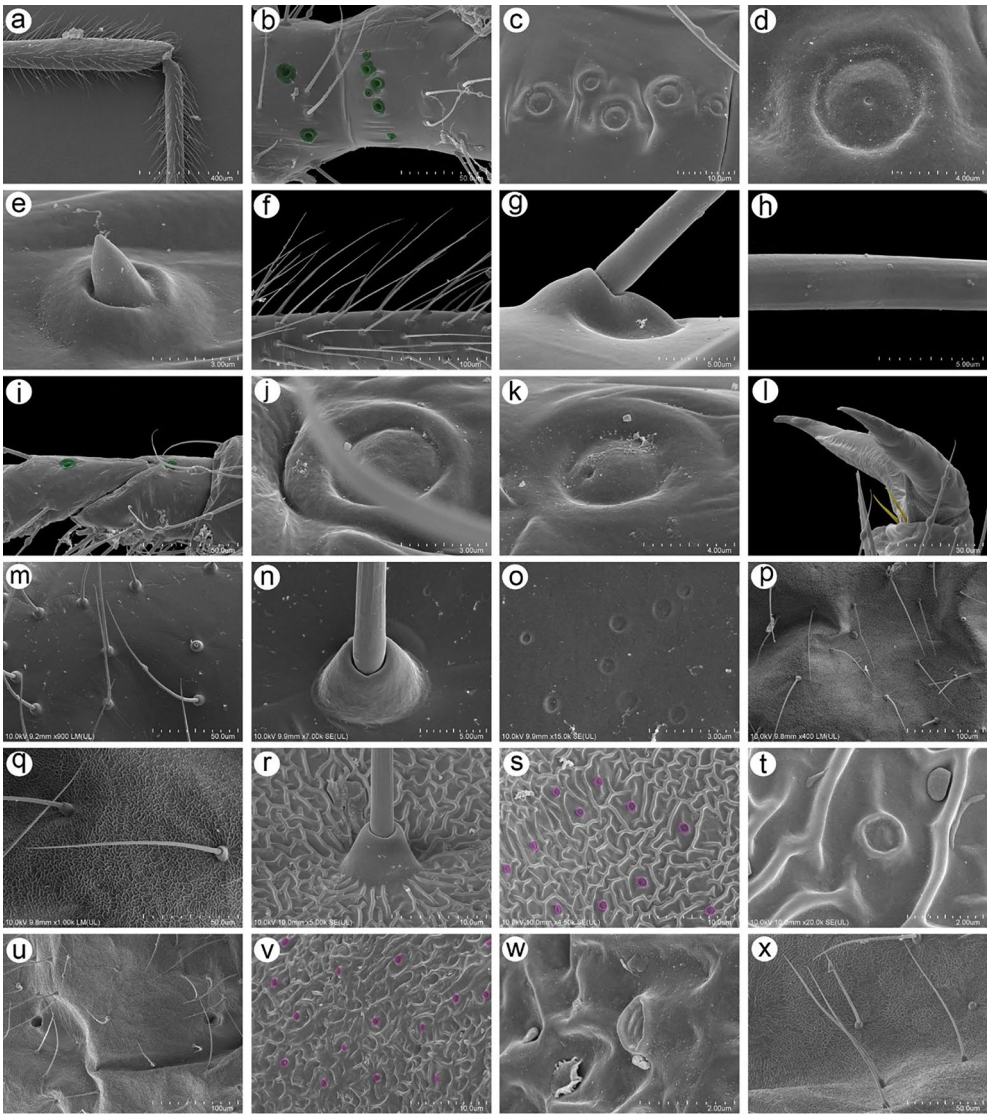

Fig. 7. Leg sensilla, cuticle surface and dorsal sensilla of apterous viviparous female of *C. pilicornis*. (**a**) hind femur and tibia densely covered with long trichoid sensilla, (**b**) inner side of hind trochanter and proximal part of hind femur with campaniform sensilla (green), (**c**) femoral campaniform sensilla of different sizes, (**d**) ultrastructure of the campaniform sensillum with visible pore in the central part of the cap, (**e**) ultrastructure of one campaniform sensillum with elevated cap, (**f**) closer look at the tibial trichoid sensilla, (**g**) ultrastructure of the socket and basal part of the trichoid sensillum, (**h**) ultrastructure of the medial part of the trichoid sensillum, (**i**) dorsal side of first segment of hind tarsus (HT I) and proximal part of second segment of hind tarsus (HT II) with campaniform sensilla (green), (**j**) ultrastructure of first segment of hind tarsus (HT I) campaniform sensillum, (**k**) ultrastructure of second segment of hind tarsus (HT II) campaniform sensillum, (l) parempodia (yellow) on the distal end of second segment of hind tarsus (HT II), (**m**) cuticle and sensilla on the head, (**n**) ultrastructure of the socket and basal part of trichoid sensillum of the head, (**o**) ultrastructure of the cuticle surface, (**p**) general view of the dorsal abdomen cuticle and sensilla (setae), (**q**) structure of the cuticle sculpture and trichoid sensillum on the abdomen, (**r**) ultrastructure of the socket and basal part of sensillum on the abdomen, (s) wax glands on the abdominal cuticle (pink), (**t**) ultrastructure of the wax gland, (**u**) general view of the lateral abdomen cuticle and sensilla, (**v**) wax glands on the lateral side of the abdomen cuticle, (**w**) ultrastructure of the wax gland, (**x**) structure of the sensilla (setae).

1. Outer side of TIBIAE III with short and rather thick setae.....2

- Outer side of TIBIAE III with fine pointed setae.....6

2. BL 3.2-6.7 mm, but usually more than 4.5 mm. Coxae black. Ultimate rostral segment IV more than 0.30 mm .....*Cinara piceae*

- BL 2.4-4.2 mm. Coxae light brown. Ultimate rostral segment IV less than 0.25 mm……....3

3. SIPH cones pale, almost concolorous with dorsal cuticle ……....*Cinara fornacula*

- SIPH cones pigmented, much darker than rest of dorsal cuticle.....4

4. ABD VII and VIII both with dark sclerotic cross-bands (sometimes divided in midline or partially fragmented)…….....5

- Dark cross-bands absent from ABD VII and VIII or only present on ABD VIII…….....6

5. URS shorter than HT II, ultimate rostral segment IV with 5-9 accessory setae……...*Cinara piceicola*

- URS longer than HT II, ultimate rostral segment IV with 9-13 accessory setae……..…..*Cinara pruinosa*

6. HT II longer than maximum diameter of SIPH cones, which are small and often rather pale...*Cinara pilicornis*

- HT II shorter than maximum diameter of SIPH cones.....7

7. FEMORA III either wholly pale or with patchy or banded pigmentation. Tibial with dark setae, often with pigmented bases. Dorsal abdominal setae often arising from small sclerites……..…… *Cinara costata*

- FEMORA III sometimes wholly pale but usually pale basally becoming dark distally. Tibial with pale or dusky setae, usually with unpigmented bases, and dorsal abdominal hairs rarely arising from small sclerites.....8

8. URS 1.1-1.5× longer than HT II……..*Cinara pruinosa*

- URS 1.1 × less than HT II ..... *Cinara braggii*

Molecular analyses

Phylogenetic analyses and species delimitation

The Bayesian Inference (BI) and Neighbour-joining analysis (NJ) inferred from the COI gene showed that multiple aphid samples were divided into five clades and were identified as the following species (Fig. 8a): *Cinara costata*, *C. fornacula*, *C. piceae*, *C. piceicola*, and *C. pilicornis*. The species delimitation methods of ABGD, ASAP and bPTP yielded five molecular operational taxonomic units (MOTUs), respectively. The pairwise distance gap approach (ABGD) with default settings (X = 0.5) suggested five species with a barcode gap distance of 3.0%. The first ASAP-score (1.5) was chosen, which provides the best-fit scenario at the threshold distance of 2.69% (JC69) with five hypothetical species. The bPTP showed five hypothetical species. The distinct separation of clades observed in the study demonstrates that the COI barcode region is an effective tool for identifying closely related species. Molecular analyses of the COI gene from *C. pilicornis* collected across various countries provide strong support for the identification of the *Cinara* species found in South Korea as *C. pilicornis*.

Genetic divergence

Genetic divergences (GDs) within all species included in this study are presented in Table 1. The intraspecific and interspecies GDs for five species (*Cinara costata*, *C. fornacula*, *C. piceae*, *C. piceicola*, and *C. pilicornis*) were analyzed using COI sequences. The intraspecific GD was analyzed with 711 comparison pairs, averaged 0.1%, and the maximum intraspecific divergence did not exceed 0.3%. The highest value of intraspecific GD was found in *C. fornacula*, with 0.3%. The interspecies GD was analyzed with 1,369 comparison pairs. The minimum interspecific GD among all five species was calculated to be 5.6% between *C. piceicola* and *C. pilicornis*, while the maximum interspecific divergence value was 11.2% (averaging 8.8%) between *C. costata* and *C. piceicola*. All species analyzed in this study exhibited a distinct barcode gap between the maximum intraspecific GD (0.3%) and the minimum interspecific GD (5.6%) in the COI gene (Fig. 8b).

Population analyses

The TCS analysis indicated that 12 haplotypes were detected from the 65 ingroup COI sequences (Fig. 9a). Haplotype distribution information for all individuals is provided in Supplementary Table 2. A total of 35 sequences of *C. pilicornis* revealed a total 6 haplotypes (Hap_1–6). All COI sequences obtained in the South Korean *C. pilicornis* population belongs to haplotype 1, and the haplotype is presumed to be an ancestral haplotype, since the haplotype is found in most region in the dataset. In the PCoA (Fig. 9b), all *C. pilicornis* species were closely clustered together, partially overlapping with each other, and this species forms a clearly different group from the other species.

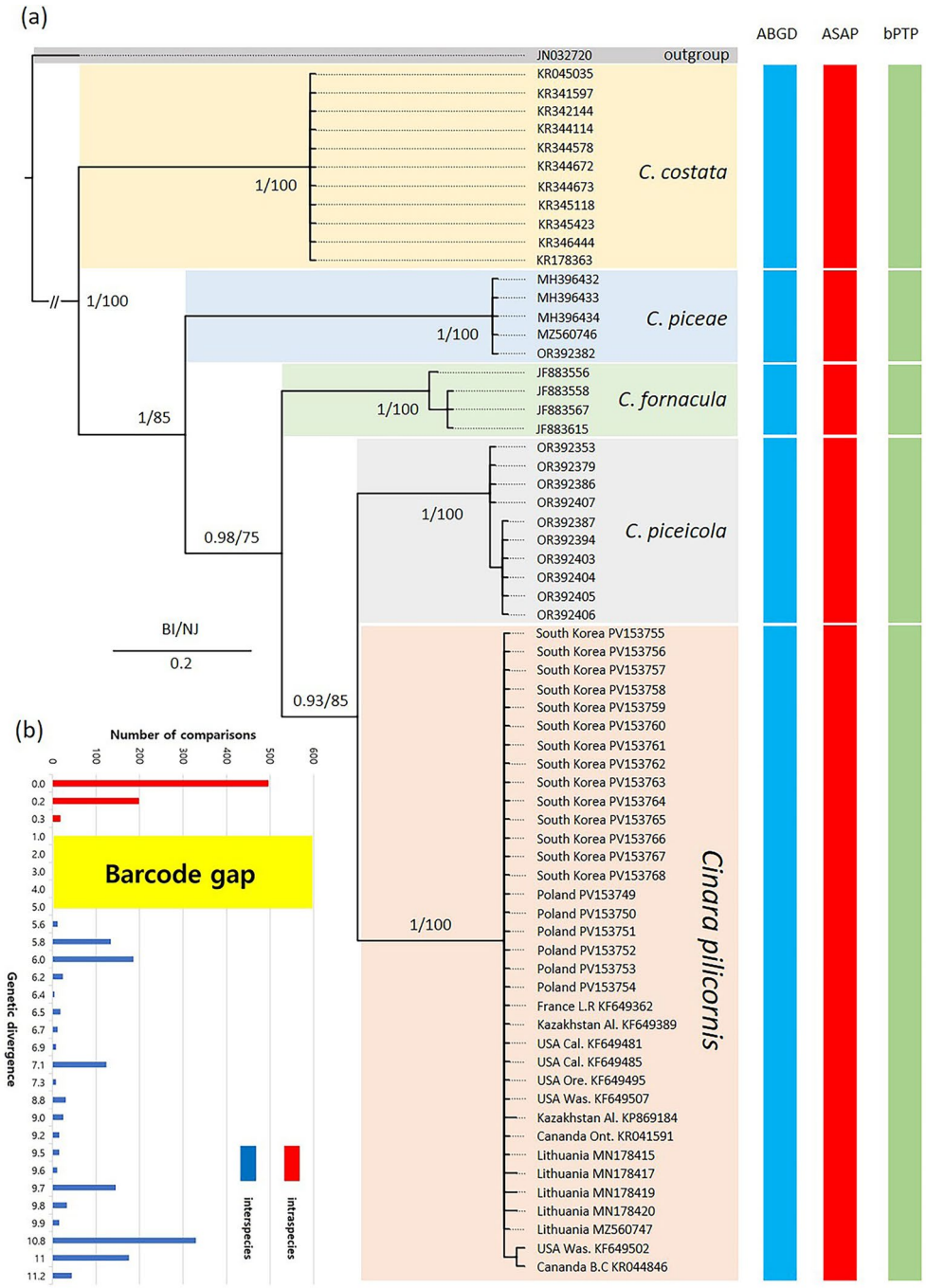

Fig. 8. Phylogenetic analyses of *Picea*-feeding *Cinara* species: (**a**) Species delimitation: each node is marked with two types of supporting value: Bayesian inference (BI) and neighbor-joining analysis (NJ), (**b**) Distribution of genetic divergences based on the Kimura 2-parameter model for COI sequences according to taxonomic levels. A total of 711 comparison pairs within the species and 1,369 comparison pairs between the species were calculated.

Climatic niche modeling

All models developed using RF and GBM with ten replications demonstrated superior performance, exceeding the criteria of TSS (>0.7) and AUC (>0.8). Consequently, all models were integrated into a final ensemble model. Among the bioclimatic variables, bio8 (Mean Temperature of the Wettest Quarter), bio19 (Precipitation of the Coldest Quarter), and bio9 (Mean Temperature of the Driest Quarter) showed the highest contributions to model performance, while the remaining variables (bio3, bio2, bio15, bio18, and bio13) were of moderate importance (Supplementary Fig. 2). The climatic suitability map for *C. pilicornis* indicates that this species has the potential to become established in temperate and subtropical regions, including Europe, North America, coastal regions of South America, and East Asia including Korea (Fig. 10).

(1) Different taxonomic levels				
Taxonomic level (No. of Comparison Pairs)		K2P Pairwise distances		
		Maximum	Minimum	Mean
Within species (711)		0.3	0.0	0.1
Between species (1,369)		11.2	5.6	8.8
(2) Intraspecific genetic divergence				
Species	Comparison pairs (CP)	Intraspecific genetic divergence		
		Maximum	Minimum	Mean
Cinara costata	55	0.0	0.0	0.0
C. fornacula	6	0.0	0.3	0.2
C. piceae	10	0.0	0.0	0.0
C. piceicola	45	0.0	0.2	0.1
C. pilicornis	595	0.3	0.0	0.1

(3) Interspecific genetic divergence				
Species	*Cinara costata*	*C. fornacula*	*C. piceae*	*C. piceicola*
C. fornacula	CP=44, 9.8 (9.6-9.8)			
C. piceae	CP=55, 11.0 (11.0-11.0)	CP=15, 9.2 (9.2-9.2)		
C. piceicola	CP=110, 11.1 (11.0-11.2)	CP=40, 6.5 (6.2-6.7)	CP=50, 8.9 (8.8-9.0)	
C. pilicornis	CP=385, 10.9 (10.8-11.0)	CP=140, 7.1 (6.9-7.3)	CP=180, 9.6 (9.0-9.9)	CP=350, 5.9 (5.6-6.2)

Table 1. Genetic divergences within all species included in this study.

Biology

For the first time in early June, two large colonies of *C. pilicornis* (12 and 17 individuals per colony) were discovered on the shoots of *Picea abies* in this study (Fig. 1 g). During early July (summer), revisiting the tree in the same location revealed that this species did not display host alternation (Fig. 1 h). Instead, it had spread to shoots of neighboring host plants, forming an additional six small colonies (2–4 individuals per colony). During summer, a small number of individuals were observed feeding on the sap from the woody parts of new shoots, and ants (*Lasius* sp.) were observed visiting aphid colonies (Fig. 1 h). No natural enemies were observed approaching these aphid colonies.

Damage

A significant amount of honeydew was observed on the sites where aphid colonies had established, as well as on the branches and leaves beneath these colonies. Moreover, black sooty mold had begun to develop on branches and leaves.

Discussion

Past and present studies on *Cinara* species feeding on *Picea*

Since aphids diversity in South Korea was first studied in 1927[24], a *Cinara* species, which feeds on the *Picea* tree, has been reported for the first time in South Korea. In 1994[25], 17 *Cinara* species feeding the sap of conifer trees (Pinaceae: *Abies*, *Cedrus*, *Larix*, and *Pinus* and Cupressaceae: *Juniperus* and *Platycladus*) were studied, and recently in 2020[26], *Cinara cedri*, an invasive species native to Europe, was reported. We began intensively monitoring aphids on imported conifer trees across South Korea in 2018. This study represents the first record of *C. pilicornis* in South Korea, expanding the known distribution of this invasive species. The integration of morphological, molecular, and ecological data in this research not only confirms the identification of *C. pilicornis* but also highlights its potential to establish and spread in the temperate regions of East Asia, including South Korea. Our findings have significant implications for biosecurity and forest management, particularly in areas where spruce trees are an integral component of native or managed ecosystems.

Morphology

In this study, we morphological redescription was based on South Korean specimens, which correspond to Haplotype 1 in our haplotype analysis. Apart from some limited comparative material from Poland, we were not able to obtain additional specimens from other regions represented in the genetic dataset. We performed

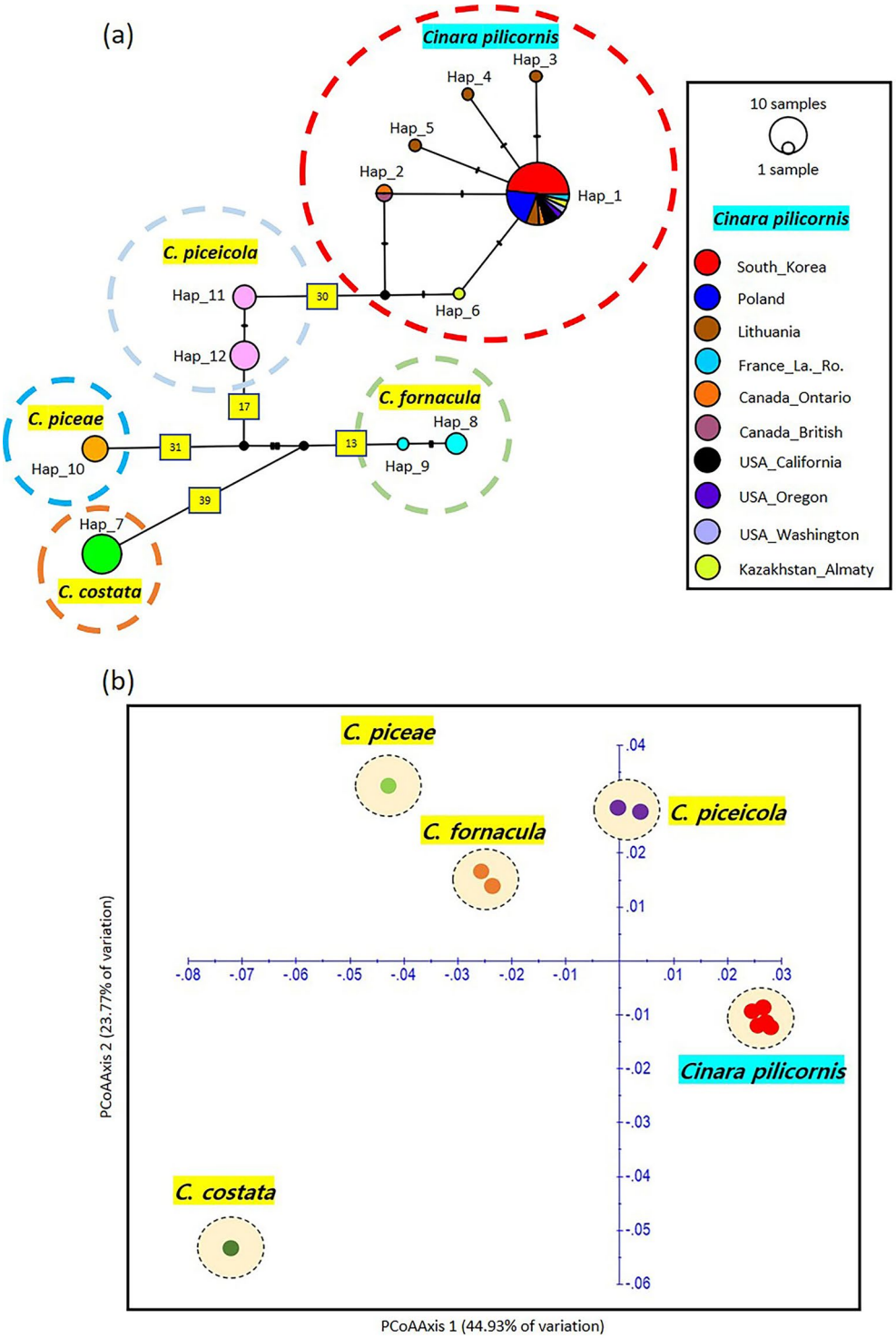

Fig. 9. Population analyses of five *Picea*-feeding *Cinara* species: (**a**) TCS network of nine haplotypes of the 65 COI sequences. The pi size is proportional to the haplotype frequency. The number in the box indicates the number of mutations. A dotted circle means the same species, (**b**) The PCoA graph was generated based on the COI haplotypes.

haplotype analysis using COI data from Genbank. The primary aim of our study is to report the occurrence and diagnostic traits of this invasive species in East Asia, especially South Korea. We think that the morphological data we present will be valuable for identifying *C. pilicornis* in other parts of Asia where it may be newly introduced, even if future work reveals morphological differences linked to geographic or haplotypic variation.

To date, comparative SEM studies on the morphology and distribution of sensilla have been conducted primarily in a few genera of Eulachnini, such as *Eulachnus*[21] and *Pseudessigella*[27,28]. However, despite *Cinara*

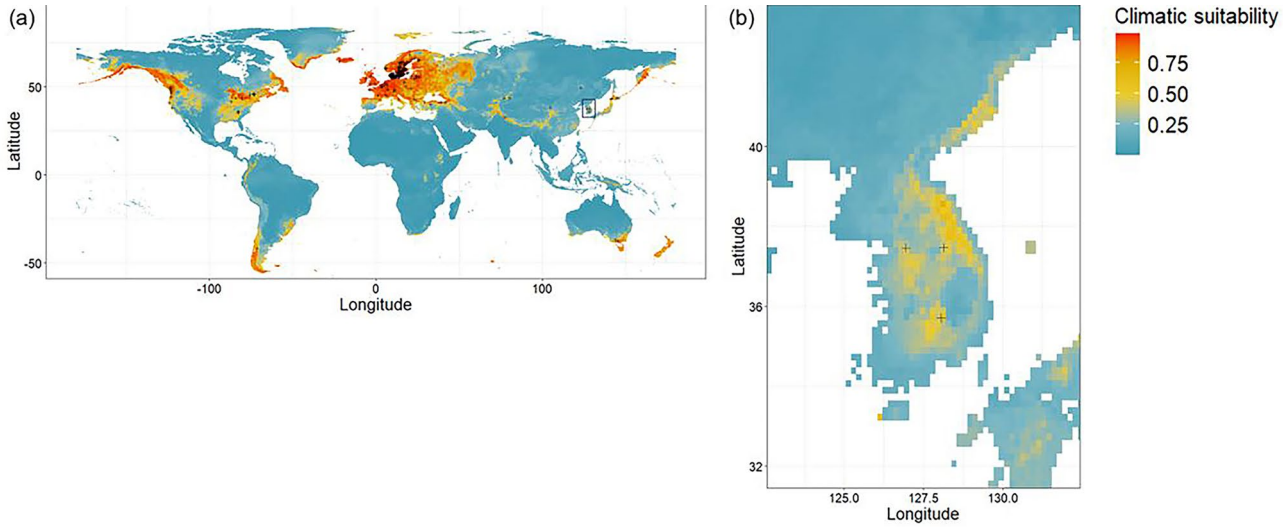

Fig. 10. Estimated climatic suitability for *Cinara pilicornis* (**a**) at the global scale and (**b**) on the Korean Peninsula. Crosses (+) indicate known presence points used in the climatic niche modeling.

being the most speciose genus within the subfamily Lachninae, comprehensive sensillar analyses across its many species remain scarce. The present study was intended as a foundational work that documents in detail the external morphology of *Cinara pilicornis*, including its antennal and mouthpart sensilla, which have not been thoroughly described before. Our aim is to provide a morphological baseline that may facilitate future comparative studies, within the subgenus *Cinara* and related subgenera. Moreover, further investigations are necessary to assess whether species formerly treated as separate genera (e.g., *Cinaria*, *Cinarella*, *Cinaropsis*) exhibit consistent sensillar differences that can be used diagnostically. At present, the lack of sufficient SEM data across a broader range of *Cinara* species precludes meaningful comparisons or the establishment of reliable diagnostic features based on sensillar morphology. However, the potential of this approach has been demonstrated in other aphid lineages. For instance, SEM-based sensillar analysis was successfully employed to resolve cryptic species boundaries in *Essigella*[29]and more recently, to infer phylogenetic relationships among higher aphid taxa[30]. In conclusion, while our current dataset does not permit a taxonomic key based on sensillar traits for *Cinara*, we think that our findings represent a necessary step toward that goal. We hope that this study will serve as a reference point for future comparative works that may enable the use of sensilla as reliable taxonomic characters in this morphologically challenging group.

Genetic homogeneity and invasion route

Molecular analyses revealed low genetic diversity among South Korean populations of *C. pilicornis*, with all specimens belonging to haplotype 1. This suggests a recent introduction event, potentially from a single source population or multiple introductions from a genetically similar region. The presence of haplotype 1 across multiple geographical regions supports the hypothesis that this haplotype may represent the ancestral lineage of *C. pilicornis*. Similar genetic bottleneck effects have been observed in other invasive aphid species, where founder effects and limited genetic variation do not hinder establishment but rather facilitate rapid population expansion[31]. The observed genetic uniformity among South Korean populations of *C. pilicornis* suggests a recent introduction, possibly through the importation of *P. abies* seedlings from Europe. This finding underscores the need to reinforce phytosanitary measures during plant importation, as identifying potential invasion pathways is critical for designing effective biosecurity strategies and preventing further spread of this invasive species.

Climatic suitability and potential invasion risk

The climatic niche modeling for *C. pilicornis* suggests that this species could potentially establish in regions beyond its currently known range, including Eastern Europe, eastern Canada, parts of South America, and the Korean Peninsula. Although New Zealand was not included in the presence dataset due to limited available records, the model identified the region as climatically suitable, which is consistent with historical observations of its establishment and spread during the 1920s[32].

However, given the host specificity of *C. pilicornis*, host availability is a prerequisite for establishment. Even in climatically suitable areas, the absence of appropriate host plants would prevent successful colonization. This highlights the importance of considering both climatic and host distributions when interpreting species distribution models for herbivores closely associated with specific hosts. In South Korea, *P. abies*, the primary host of *C. pilicornis*, is an introduced species that has been planted in mountainous afforestation areas or gardens for during a century, while several native *Picea* taxa are confined to limited high-altitude areas[33,34]. Considering the estimated climatic suitability of *C. pilicornis*, high-altitude zones in Korea or areas where *P. abies* may represent potential habitats where this aphid could occur.

The modeled climatic suitability broadly overlaps with the global distribution of *P. abies* and other species within the genus *Picea* (Fig. 10; Supplementary Fig. 3), which are known host plants of *C. pilicornis*. This spatial correspondence may indicate that the climatic preferences of the aphid partially reflect the ecological conditions favorable for its hosts. Although our model estimates a correlative climatic niche based solely on abiotic variables, the overlap with host distribution suggests that host availability may be indirectly represented due to shared climatic constraints. However, since host distribution was not explicitly incorporated into the model, its influence cannot be isolated, and the biological requirements for establishment should be interpreted with caution.

Another consideration when interpreting the estimated climatic suitability for *C. pilicornis* is that climatic niche modeling has been applied here to a species that is expanding its range. The PA points used in the model do not distinguish between areas that are truly unsuitable for establishment and those that have not yet been reached due to limited dispersal ability or geographic barriers. Therefore, our results provide a broad approximation of potentially suitable climatic regions but may underestimate the actual extent of favorable conditions. To more accurately assess the invasion risk of this species, future research should incorporate more detailed information on its climatic tolerances.

Quarantine and management implications

The designation of *C. pilicornis* as a quarantine pest by the Animal and Plant Quarantine Agency of South Korea underscores the necessity of stringent phytosanitary measures. Given its potential economic impact on forestry and its ability to spread via international plant trade, a comprehensive monitoring program should be established at ports of entry and in regions with high *Picea* cultivation. Early detection efforts should integrate molecular diagnostic tools to differentiate *C. pilicornis* from other *Cinara* species, particularly in mixed-species aphid infestations. It is inferred that the environmental adaptability of aphids may be enhanced by the wax secreted from the wax glands of these aphids. Additional research should be conducted on the correlation between aphid wax and the actual behavior after invasion into other environments. This species causes serious damage to host plants, manifesting in the form of reduced honey production, black sooty mold growth, and reduced photosynthetic efficiency, and has the potential to pose a significant threat to natural forest ecosystems and commercial forestry. Long-term studies are needed to monitor the genetic diversity and adaptability of *C. pilicornis* populations in South Korea. Further studies on ecological interactions, including host specificity and seasonal dynamics, will provide the South Korean government and the forestry agency with insights needed to improve management strategies for this invasive species. Combining early detection, biological control, and public engagement may effectively mitigate the spread and impacts of *C. pilicornis* in South Korea. In particular, monitoring of endemic *Picea* species in national parks near the areas where the invasive species has been detected should be prioritized to prevent further damage to native conifer populations on the South Korea, and studies on natural enemies should be conducted urgently for biological control.

Materials and methods

Collection and identification

In June 2024, *C. pilicornis* was discovered on Norway spruce (*Picea abies*) by M. Lee in Gangwon, Gyeongsangnam Province region, and Seoul (Fig. 1a-c; Supplementary Fig. 1). Photographs were taken with a Canon 70D camera equipped with extension rings. The aphid samples were preserved in 95% ethanol and slide glass specimens were mounted in Canada balsam, following a previously published method[7]. Specimens were identified as the spruce shoot aphid, *C. pilicornis*, according to the taxonomic key[7]. Measurements and digital images were taken using a Leica DMC 5400 (Leica Z16 APO) and a Leica DM 4000B camera (Active Measure version 3.0.3; Mitani Co. Ltd., Japan). Abbreviations used for descriptions are as follows: ANT, antennae; ANT I, ANT II, ANT III, ANT IV, ANT V, BASE, and PT, antennal segments I, II, III, IV, V, base of VI, and processus terminalis of antennomere VI respectively; BL, body length; HW, maximum head width across compound eyes; MaxW, maximum body width; GP, genital plate; HT I, first segment of hind tarsus; HT Ib, basal length of HT I; HT Id, dorsal length of HT I; HT Iv, ventral length of HT I; HT II, second segment of hind tarsus; SIPH, siphunculi; URS, ultimate rostral segment (segment IV + V); ABD I–VIII, abdominal tergites I–VIII, respectively; FEMORA III, hind femora; TIBIAE III, hind tibiae; FWL, forewing length; HWL, hind wing length. Slide specimens are deposited at the College for Agriculture and Life Sciences, Seoul National University Seoul, Korea (SNU) and in the SEM laboratory of the Institute of Biology, Biotechnology, and Environmental Protection, University of Silesia in Katowice (Katowice, Poland).

Material examined

Apterous viviparous female. 5, South Korea, Gangwon-do, Hoengseong-gun, Anheung-myeon, on *Picea abies*, 7.vi.2024, leg. M. Lee, [voucher, 240607-LMH-1, 1–5] (SNU); 3, South Korea, Seoul, Gwanak-gu, Gwanak-ro 1, on *P. abies*, 22.vi.2024, leg. M. Lee, [voucher, 240622-LMH-1, 1–3] (SNU); 2, South Korea, Gangwon-do, Hoengseong-gun, Anheung-myeon, on *P. abies*, 12.vii.2024, leg. M. Lee, [voucher, 240712-LMH-1, 1, 2] (SNU). 2, South Korea, Gyeongsangnam-do, Geochang-gun, Gajo-myeon, on *Picea abies*, 20.vii. 2024, leg. M. Lee, [voucher, 240720-LMH-1, 1, 2] (SNU).

Alate viviparous female. 1, South Korea, Gangwon-do, Hoengseong-gun, Anheung-myeon, on *P. abies*, 7.vi.2024, leg. M. Lee, [voucher, 240607-LMH-1] (SNU); 1, South Korea, Seoul, Gwanak-gu, Gwanak-ro 1, on *P. abies*, 22.vi.2024, leg. M. Lee, [voucher, 240622-LMH-1] (SNU).

Scanning electron microscopy

Samples used in this study were collected directly in the field and kept in 80% ethanol for several days. Dehydration of the ethanol-preserved four samples was performed using an ethanol series of 80, 90, 96% and two changes of absolute ethanol for 10 min each. From absolute alcohol the samples were transferred to pure chloroform and stored at room temperature for 24 h. Dehydrated and cleaned specimens were dried using the Leica EM CPD 300 auto critical point dryer (Leica Microsystems, Vienna, Austria). Dry samples were mounted on aluminum stubs with double sided adhesive carbon tape and sputter coated with a 30 nm layer of gold in a Quorum 150 T ES Plus sputter coater (Quorum Technologies Ltd, Laughton, East Sussex, UK). The specimens were imaged by the Hitachi SU8010 field emission scanning electron microscope FESEM (Hitachi High–Technologies Corporation, Tokyo, Japan) at 10 kV accelerating voltage with a secondary electron detector (ESD) in the SEM laboratory of the Institute of Biology, Biotechnology, and Environmental Protection, University of Silesia in Katowice (Katowice, Poland).

Molecular protocol

Genomic DNA was extracted from individual samples collected from each colony using the DNeasy Blood & Tissue kit (Qiagen, Dusseldorf, Germany) following modified manufacturer protocols. A 658 bp segment of the cytochrome oxidase I gene (COI) was amplified using the following primer sets: LepF 5′- ATTCAAC CAATCATAAAGATATTGG-3′ and LepR 5′ TAAACTTCTGGATGTCCAAAAAATCA-3′. Polymerase chain reaction (PCR) was performed using AccuPower PCR Premix (Bioneer, Daejeon, Rep. of Korea) in 20 µl reaction volumes. The amplification protocol consisted of an initial denaturation at 94 °C for 3 min; followed by 35 cycles at 94 °C for 30 s, an annealing temperature of 45.2 °C for 30 s, extension at 72 °C for 1 min, and the final extension step at 72 °C for 5 min. PCR products were checked in 1.5% agarose gel, purified, and sequenced at Bionics, Inc. (Seoul, Republic of Korea).

Molecular analyses

Sequence analysis and genetic divergence

In total, 65 COI sequences of *Picea*-feeding *Cinara* spp. were analyzed, including 20 sequences generated in this study and 45 sequences retrieved from GenBank. *Lachnus tropicalis* (GenBank accession number: JN032720) was used as an outgroup. The sequences were deposited in GenBank (accession numbers PV153749 to PV153768) and are detailed in Supplementary Table 2. Raw sequences were assembled and edited using SeqMan Pro ver. 7.1.0 (DNASTAR, Inc., Madison, Wisconsin, USA). Sequence alignment was performed using MEGA 7[35]. Intra and interspecific pairwise genetic distances between the groups were calculated using the pairwise distance method, which is based on the Kimura 2-parameter (K2P) mo.

Phylogenetic analysis and species delimitation

Phylogenetic analyses were conducted using Bayesian inference (BI) and neighbor-joining analysis (NJ). The BI analysis was conducted using MrBayes v.3.2.6[36], with 10 million Markov chain Monte Carlo (MCMC) generations, and trees were sampled every 1,000 generations. A burnin of 25% of the sampled trees was applied to ensure adequate mixing of the MCMC chain with the best partition scheme and best-ft substitution models found by PARTITION-FINDER2[37]. The result was visualized using FIGTREE v.1.4.4[38]. The NJ analysis was conducted using MEGA 7, which is based on the Kimura 2-parameter (K2P) model[35]. We followed three DNA-based species delimitation methods proposed by Wieczorek & Sawka[39]: Automatic Barcode Gap Discovery (ABGD), Assemble Species by Automatic Partitioning (ASAP), and Bayesian implementation of the PTP (bPTP). ABDG was performed using the ABDG web server (https://bioinfo.mnhn.fr/abi/public/abgd/abgdweb.htm, accessed on 15 July, 2024) and ASAP was performed using the ASAP web server (https://bioinfo.mnhn.fr/abi/public/asap/, accessed on 15 Jul,. 2024) with alignment of sequences as an input file. bPTP was performed with the PTP web server (https://species.h-its.org, accessed on 15 July 2024) using the Bayesian inference result file from the previous analysis as an input.

Population genetic analyses

The identification of variable and parsimoniously informative sites and the number of haplotypes (h) were estimated using DnaSP v6.12.03[40]. Based on the haplotype list generated from DnaSP v6.12.03, the number of private haplotypes unique to each population was determined (Supplementary Table 2). Haplotype data were generated in DnaSP v6.12.03 to identify the unique haplotypes. A statistical parsimony network was constructed using the TCS method[41] as implemented in PopART[42] to visualize haplotype relationships. To further evaluate and visualize the geographic genetic structure among the populations, principal coordinates analysis (PCoA) was conducted using the DARwin 6.0.9 program[43].

Climatic niche modeling

Occurrence data for *C. pilicornis* were obtained from the Global Biodiversity Information Facility (GBIF) and from presence records reported in published studies. GBIF data were accessed on 12 May 2025 (https://doi.org/10.15468/dl.m4gsfr). Among a total of 1,112 records, those flagged with major spatial or taxonomic issues (such as invalid coordinate precision, mismatched country-coordinate information, invalid spatial footprints, or fuzzy taxon matches) were removed based on the issue field provided by GBIF. Only records without such flags were retained for subsequent analyses. Duplicate records and those lacking geocoordinates were then excluded, resulting in 208 records. The GBIF records were predominantly distributed in the western part of Europe. An additional 31 presence records were obtained from published sources and from field investigations conducted in Korea and Poland (Supplementary Table 3). In total, 239 presence records were compiled for subsequent analyses.

To reduce spatial autocorrelation, spatial thinning was applied to the presence points of *C. pilicornis*. The original 239 points were evaluated with point pattern analysis based on nearest-neighbor distances using the *spatstat* package in R 4.4.2. The results showed a significantly clustered distribution within the spatial window defined by the maximum and minimum values of longitude and latitude (Monte-Carlo simulation; $p < 0.05$). Spatial thinning was then performed based on the expected distance under the assumption of complete spatial randomness (CSR), as determined by the nearest-neighbor distance test. After thinning, a total of 178 presence points were retained for analysis.

Pseudo-absence (PA) points were sampled to provide contrast to presence points and allow the model to identify suitable climatic conditions. its spatial pattern in relation to bioclimatic variables. For PA sampling, a spatial buffer of 2° (decimal degrees) was created around each presence point, ensuring that PA points were sufficiently distant from presence points[44]. PA points were randomly sampled from the masked study area raster, which excluded the buffered presence areas, with the number of PA points matching the number of presence points[44]. The resulting PA datasets were combined with the presence data to create the final inputs for modeling. This sampling process was replicated ten times, producing ten occurrence datasets with identical presence points but varying PA points.

Bioclimatic variables with a 10 arc-minute spatial resolution were obtained from the WorldClim version 2.1 database (https://www.worldclim.org/). These variables included 19 standard bioclimatic layers (bio1 to bio19), representing temperature and precipitation-based gradients. To reduce multicollinearity, a correlation-based variable selection approach was applied using the *vifcor* function from the *usdm* package in R 4.2.2[45]. Variables with a pairwise correlation exceeding 0.85 were identified, and among highly correlated pairs, the variable with the higher variance inflation factor (VIF) was iteratively removed. This process resulted in a final selection of eight bioclimatic variables: bio2 (Mean Diurnal Range), bio3 (Isothermality), bio8 (Mean Temperature of the Wettest Quarter), bio9 (Mean Temperature of the Driest Quarter), bio13 (Precipitation of the Wettest Month), bio15 (Precipitation Seasonality), bio18 (Precipitation of the Warmest Quarter), and bio19 (Precipitation of the Coldest Quarter).

To estimate the climatic niche of *C. pilicornis*, two tree-based modeling algorithms, Random Forest (RF) and Gradient Boosting Machine (GBM), were employed to address nonlinear relationships and interactions among variables. Models were trained using the *BIOMOD_Modeling* function with the "bigboss" strategy in the *biomod2* package. For each of the ten occurrence datasets, models were built using 70% of the data for training and 30% for validation. A total of 20 models (2 algorithms × 10 datasets) were constructed. Model performance was evaluated using the true skill statistic (TSS) and the area under the receiver operating characteristic curve (AUC). TSS values range from − 1 to 1 and are calculated as sensitivity + specificity − 1, while AUC ranges from 0.5 (random prediction) to 1 (perfect discrimination).

By averaging the predictions (scaled presence probabilities ranging from 0 to 1), an ensemble prediction model was built. The base models exhibiting superior performance (TSS > 0.7 and AUC > 0.8) were selected and averaged to generate ensemble predictions using the biomod2 package in R 4.2.2[45]. Variable contributions in the final model were assessed using permutation importance, which quantifies the impact of each variable by randomly permuting its values and evaluating changes in model performance. To ensure robustness, the permutation importance scores were calculated for each variable across ten replicates and averaged. Finally, the ensemble model was projected onto geographical space to identify the potential distribution of *C. pilicornis*.

Data availability

Data Availability: Data is provided within supplementary information files.

Received: 23 February 2025; Accepted: 18 July 2025
Published online: 08 August 2025

References

1. Pyšek, P. et al. Contrasting patterns in the invasions of European terrestrial and freshwater habitats by alien plants, insects and vertebrates. *Glob Ecol Biogeogr*. **19**, 317–331 (2010).
2. Hulme, P. E. Climate change and biological invasions: evidence, expectations, and response options. *Biol Rev*. **92**, 1297–1313 (2017).
3. Kim, S., Jung, J. K., Park, I., Lee, B. W. & Kim, Y. H. Integrated identification and genetic diversity of potentially invasive clearwing moths (Lepidoptera: cossoidea: Sesiidae) in Korea. *Insects* **15**, 79 (2024).
4. Neto, A. C. et al. First record of the invasive leafhopper *Sophonia orientalis* in Mainland Portugal. *J Pest Sci*. **94**, 241–249 (2021).
5. Normark, B. B. Molecular systematics and evolution of the aphid family Lachnidae. *Mol Phylogenet Evol*. **14**, 131–140 (2000).
6. Favret, C. & Voegtlin, D. J. A revision of the *Cinara* species (Hemiptera: Aphididae) of the united States Pinyon Pines. *Ann Entomol Soc Am*. **97**, 1165–1197 (2004).
7. Favret, C. & Aphid Taxon Community, eds. Blackman & Eastop's Aphids on the World's Plants, version 1.0. Accessed at (2025). https://aphidsonworldsplants.info/ on (3 May 2025).
8. Favret, C. *Aphid Species File*. Version 5.0/5.0. Available at: http://Aphid.SpeciesFile.org (2025).
9. Ayache, S. et al. A new species, Cinara tellenica Binazzi F. et strangi (Aphididae: Lachninae) associated with cedrus Atlantica in the tell atlas of Algeria. *Bull. Insectol*. **73**, 275–283 (2020).
10. Forbes, A. R. & Chan, C. K. List of British Columbia aphids. *IV J. Entomol Soc Br Columb*. **73**, 57–63 (1976).
11. Inouye, M. Revision of the conifer aphid fauna of Japan (Homoptera: Lachnidae). *Bull Gov for Exp Stn*. **228**, 57–102 (1970).
12. Eastop, V. F. A taxonomic review of the species of *Cinara* Curtis occurring in Britain (Hemiptera: Aphididae). *Bull Br Mus Nat Hist (Entomol)*. **27**, 103–186 (1972).
13. Carrillo, R. Aphidoidea de Chile II. *Agro Sur*. **5**, 109–114 (1977).
14. Ghosh, A. K. *The Fauna of India and Adjacent Countries. Homoptera, Aphidoidea. Part 2. Subfamily Lachninae*167 (Zoological Survey of India, 1982). Calcutta.
15. Sunde, R. G. New records of plant pests in new Zealand 4. 7 aphid species (Homoptera: Aphidoidea). *N. Z. J Agric Res*. **27**, 575–579 (1984).

16. Zhang, G., Zhang, W. & Zhong, T. Studies on Chinese species of *Cinara* Curtis and descriptions of new species (Homoptera: Lachnidae). *Tung Wu Hsueh Chi Kan*. **10**, 121–141 (1993).
17. Delfino, M. A. & Binazzi, A. Áfidos de coníferas En La Argentina (Hemiptera: Aphididae). *Rev Soc Entomol Argent*. **61**, 27–36 (2002).
18. Toper Kaygin, A. & Çanakçioğlu, H. Contributions to the knowledge of conifer aphid fauna in Turkey and their zoogeographical distribution. *Anz Schädlingskd*. **76**, 50–56 (2003).
19. Novgorodova, T. A. & Stekolshchikov, A. V. A contribution to the aphid (Homoptera: Aphidinea) fauna of the Kurgan Province. *Zoosyst Ross* **22**, 230–246 (2013).
20. Animal and Plant Quarantine Agency. (2025). Available at: https://www.qia.go.kr/ (Accessed: 3 January 2025).
21. Kanturski, M., Kajtoch, Ł. & Wieczorek, K. European species of the aphid genus *Eulachnus* Del guercio, 1909 (Hemiptera: aphididae: Lachninae): revision and molecular phylogeny. *Zootaxa* **4356**, 1–81 (2017).
22. Kaszyca-Taszakowska, N. & Depa, Ł. Microbiome of the aphid genus *Dysaphis* Börner (Hemiptera: Aphidinae) and its relation to ant attendance. *Insects* **13**, 1089 (2022).
23. Kaszyca-Taszakowska, N., Kanturski, M. & Depa, Ł. Perianal structures in non-myrmecophilous aphids (Hemiptera, Aphididae). *Insects* **14**, 471 (2023).
24. Okamoto, H. & Takahashi, R. Some Aphididae from Corea. *Ins Mats*. **1**, 130–148 (1927).
25. Lee, W. K., Seo, H. Y. & Hwang, C. Y. A taxonomic study on Lachnidae (Homoptera, Aphidoidea) of Korea. *Korean J Syst Zool*. **10**, 157–187 (1994).
26. Lee, J. et al. One new record of the genus *Cinara* curtis, 1835 (Hemiptera: aphididae: Lachninae) from Korea. *J Asia-Pac Biodivers*. **13**, 465–469 (2020).
27. Kanturski, M., Akbar, S. A. & Favret, C. The Bhutan pine aphid *Pseudessigella* brachychaeta Hille Ris Lambers (Hemiptera: aphididae: Lachninae) from India reveals the hitherto unknown oviparous female and Dwarfish male. *Zoological Stud.* **56**, 12 (2017).
28. Kanturski, M., Akbar, S. A. & Favret, C. Morphology and sensilla of the enigmatic Bhutan pine aphid Pseudessigella brachychaeta Hille Ris Lambers (Hemiptera: Aphididae) – A SEM study. *Zool. Anz.* **266**, 1–13 (2017).
29. Thery, T., Kanturski, M. & Favret, C. Molecular phylogenetic analysis and species delimitation in the pine needle-feeding aphid genus *Essigella* (Hemiptera: sternorrhyncha: Aphididae). *Insect Syst. Divers.* **2**, 1–15 (2018).
30. Kanturski, M., Lee, Y. & Kim, H. Phylogenetic reconstruction of Tuberolachnini and Lachninae (Insecta, Hemiptera): morphological and molecular analyses revealed a new tribe. *Front. Zool.* **21**, 29 (2024).
31. Sunnucks, P., Hales, D. F. & Simon, J. C. Evolution of an aphid clonal lineage: genetic variation and clonal selection within *Myzus persicae*. *Evolution* **51**, 490–502 (1997).
32. Zondag, R. *Elatobium abietinum* (Walker) (Hemiptera: Aphididae). Spruce aphid. *N. Z. For. Serv., For. Timber Insects N. Z.* 54 (1983).
33. Choi, H. S., Ryu, K. O., Kwon, Y. R. & Kwon, H. Y. Growth performance of 27-year-old Norway Spruce (*Picea abies*) at four plantations in Korea. *J Korean for Soc*. **96**, 145–150 (2007).
34. Kong, W. S. Biogeography of native Korean Pinaceae. *Korean Geog Soc*. **41**, 73–93 (2006).
35. Kumar, S., Stecher, G. & Tamura, K. MEGA7: Molecular evolutionary genetics analysis version 7.0 for bigger datasets. *Mol Biol Evol*. **33**, 1870–1874 (2016).
36. Ronquist, F. et al. MrBayes 3.2: efficient bayesian phylogenetic inference and model choice across a large model space. *Syst Biol*. **61**, 539–542 (2012).
37. Lanfear, R. et al. PartitionFinder 2: new methods for selecting partitioned models of evolution for molecular and morphological phylogenetic analyses. *Mol Biol Evol*. **34**, 772–773 (2016).
38. Rambaut, A. & FigTree a Graphical Viewer of Phylogenetic Trees. *Institute of Evolutionary Biology*, *University of Edinburgh*. (2009). http://tree.bio.ed.ac.uk/sofware/fgtree/
39. Wieczorek, K. & Sawka-Gądek, N. D. N. A. Barcoding and molecular phylogenetics revealed a new cryptic bamboo aphid species of the genus *Takecallis* (Hemiptera: aphidiidae). *Appl Sci*. **13**, 7798 (2023).
40. Rozas, J. et al. DnaSP 6: DNA sequence polymorphism analysis of large data sets. *Mol Biol Evol.* **34,** 3299–3302 (2017).
41. Clement, M., Posada, D. & Crandall, K. A. TCS: a computer program to estimate gene genealogies. *Mol Ecol.* **9**, 1657–1660 (2000).
42. Leigh, J. W. & Bryant, D. Popart: full-feature software for haplotype network construction. *Methods Ecol Evol*. **6**, 1110–1116 (2015).
43. Perrier, X., Jacquemoud-Collet, J. P. & DARwin software, available at, (2006). https://darwin.cirad.fr/Darwin
44. Barbet-Massin, M., Jiguet, F., H Albert, C. & Thuiller, W. Selecting pseudo-absences for species distribution models: how, where and how many? *Methods Ecol. Evol.* **3**, 327–338 (2012).
45. R Core Team. R: A Language and Environment for Statistical Computing. R0020Foundation for Statistical Computing, Vienna, Austria. (2021).

Acknowledgements

This work was supported by the Ministry of Education of the Republic of Korea and the National Research Foundation of Korea (NRF-RS-2025-00561722), supported by a National Research Foundation of Korea (NRF) grant funded by the Korea government (MSIT) (No. RS-2024-00405751), supported by the Basic Science Research Program through the National Research Foundation of Korea (NRF), funded by the Ministry of Education (NRF2020R1I1A2069484). Additional partial support was provided by the National Institute of Forest Science, Korea (Project No. FE0703-2022-01).

Author contributions

ML, MK, M-JK, AG, and SL designed the study. ML collected all the materials and wrote the manuscript. MK, AG conducted the SEM study and wrote the manuscript. M-JK studied climatic niche modeling and wrote the manuscript. SL supervised the whole process. All four authors revised the manuscript and confirmed the final version.

Declarations

Competing of interest

The authors declare that they have no known competing financial interests or personal relationships that could have appeared to influence the work reported in this paper.

Additional information

Supplementary Information The online version contains supplementary material available at https://doi.org/10.1038/s41598-025-12656-6.

Correspondence and requests for materials should be addressed to S.L.

Reprints and permissions information is available at www.nature.com/reprints.

Publisher's note Springer Nature remains neutral with regard to jurisdictional claims in published maps and institutional affiliations.